AD-A090 392 ARMY ARMAMENT RESEARCH AND DEVELOPMENT COMMAND DOVER NJ F/G 9/2
INTERIOR BALLISTIC MODELING FOR BLANK AMMUNITION,(U)
JUN 80 S GOLDSTEIN

UNCLASSIFIED NL

END
DATE FILMED
11-80
DTIC

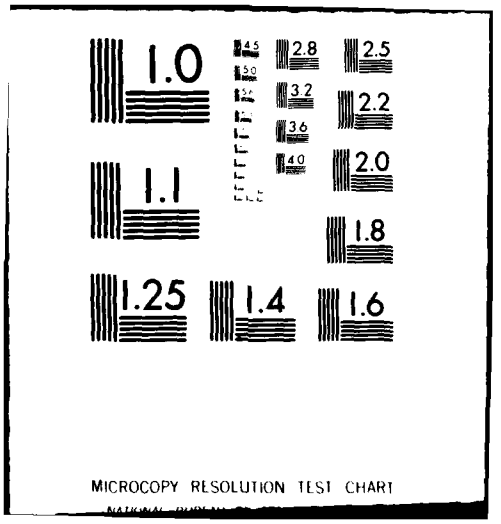
1.0
1.1
1.25
1.4
1.6
1.8
2.0
2.2
2.5
2.8
3.2
3.6
4.0
MICROCOPY RESOLUTION TEST CHART

GOLDSTEIN

INTERIOR BALLISTIC MODELING FOR BLANK AMMUNITION

SIDNEY GOLDSTEIN, MR.
U. S. ARMY ARMAMENT RESEARCH AND DEVELOPMENT COMMAND
DOVER, NEW JERSEY 07801

JUN 1980

The 1973 Yom Kipper War emphasized that adequate field training was essential for an effective modern mechanized army. There evolved, therefore, the requirement [1] to fire the .50 caliber M2HB and M85 machine guns during training exercises. As a result, blank ammunition for .50 cal weapons is currently being developed as part of the Multiple Integrated Laser Engagement System (MILES) program. This paper describes a computer model which would aid in the design of the ammunition and Blank Firing Attachment (BFA) for these systems.

EXPERIMENTAL PROCEDURE

Weapon Cycling

The .50 cal M85 machine gun was chosen as an example. Figure 1 depicts the functioning of blank ammunition in this weapon, which is recoil operated.

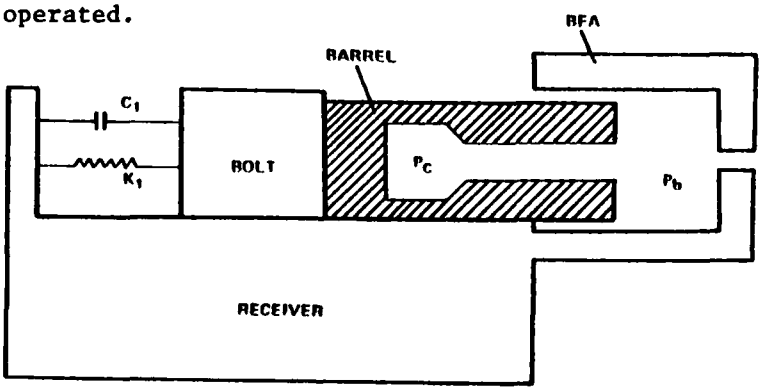

Figure 1. Bolt-Barrel Recoil.

Burning propellant in the chamber produces a pressure P_c. At some point in time, the mouth of the cartridge case opens and gas flows through the barrel producing pressure P_b in the BFA. Chamber pressure in the breech and BFA pressure on the muzzle of the barrel accelerate the bolt and barrel.

The bolt and barrel initially act as a single body during cycling of the weapon. But within a few milliseconds an accelerator separates the bolt from the barrel, and the weapon cycles independent of the gas pressure in the chamber and BFA. This model is concerned only with interior ballistics during the time the bolt and barrel remain in contact, where K_1 is the effective spring constant and C_1 is the spring damping constant.

Computer time-displacement for the bolt and barrel of the M85 machine gun when ball ammunition is fired [2] has been obtained. The bolt-barrel contact time lasts only a few milliseconds.

Ball Ammunition Performance

Pressure-time traces .50 cal M33 ball cartridge were taken at the chamber, case mouth and middle of the barrel locations. Peak force due to chamber pressure was about 10,000 lbs; ballistic cycle lasted about 2 to 3 milliseconds; and impulse was 10-11 lb-sec. The blank ammunition and BFA should be capable of duplicating this performance.

Test Set-Up

Because it was too difficult to modify the receiver in the M85 machine gun, a heavy-walled .50 cal test barrel was modified instead, and BFA simulator constructed to obtain pressure traces of .50 cal blank ammunition. Pressure stations were drilled at mid-chamber (P_c), case mouth (P_{cm}), midbarrel (P_{mb}), and the BFA (P_b) (Figure 2).

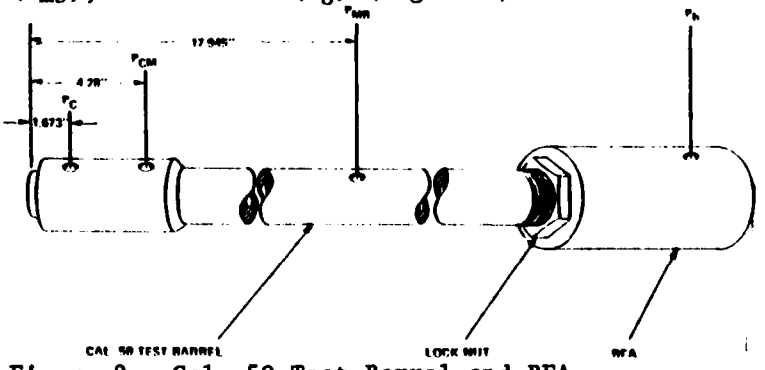

Figure 2. Cal .50 Test Barrel and BFA.

(88)

A

Shock Waves

Examination of the pressure-time traces for the chamber, midbarrel, and BFA (Figures 3, 4, and 5) showed shock waves occurring between the chamber and BFA.

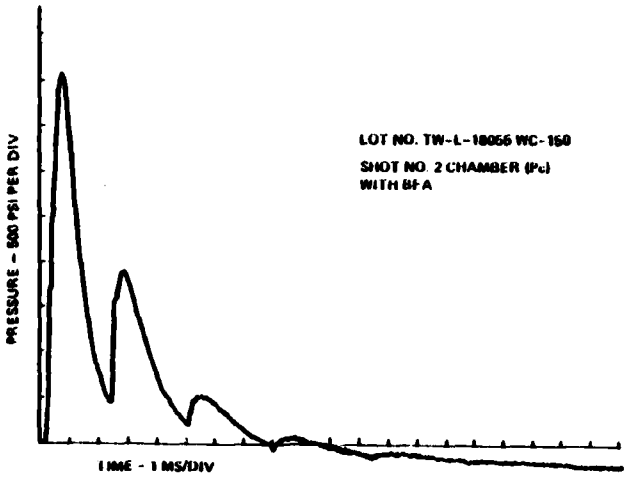

Figure 3. Chamber Pressure Versus Time.

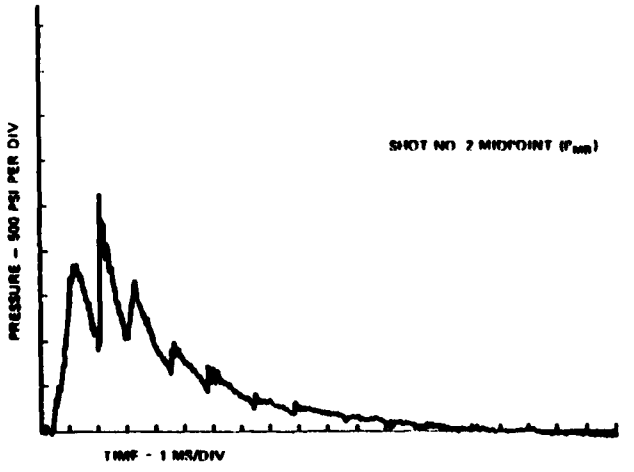

Figure 4. Midbarrel Pressure Versus Time.

89

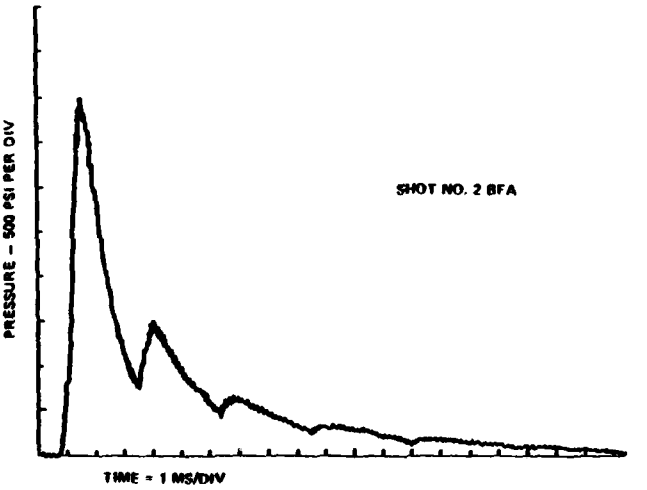

Figure 5. BFA Pressure Versus Time.

Further examination of the first return shock wave, however, indicates it does not occur immediately upon arrival of the leading shock at the BFA, but about 1 millisecond afterwards (Figure 6). Meanwhile, shock wave theory [3] states that a shock wave forms at the muzzle as soon as

$$\frac{P_b}{P_e} > \frac{2\gamma M_e^2 - \gamma + 1}{\gamma + 1} = r_{crit.} \qquad (1)$$

where M_e is the Mach number of the gas at the muzzle and γ is its ratio of specific heat.

(90)

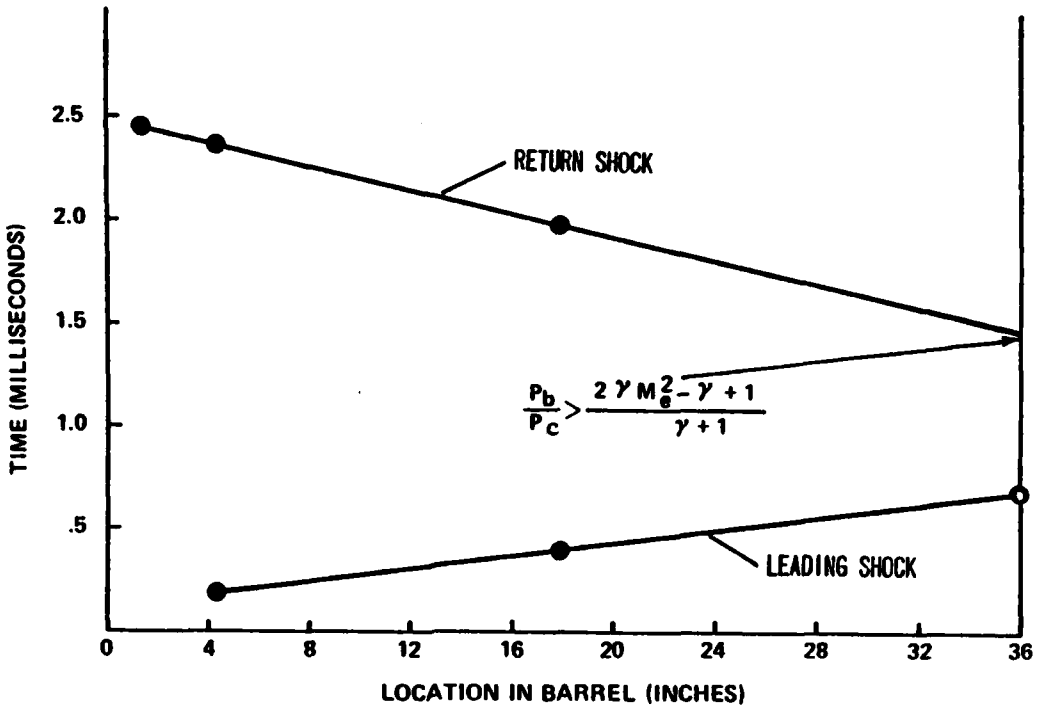

Figure 6. Shockwave Location Versus Time.

This computer program monitors the ratio P_b/P_e, and when it becomes larger than r_{crit} the gas flow to the BFA is cut off. The pressure ratio across the leading shock [4, 5] wave depends on the ratio of chamber pressure to ambient pressure at the case-mouth opening, on the ratio of the speed of sound in the gas to the speed of sound in the air, and on the values of γ in both gases (propellant gas and air).

THEORETICAL MODEL

Three Phases

Propellant combustion and gas flow occur in three separate phases (Figure 7). Phase I occurs in the chamber and includes:

a. Isochoric or constant volume combustion until the mouth of the cartridge case opens.
b. Quasisteady combustion and two-phase flow.
c. Flame quenching.
d. Quasisteady isentropic flow through a converging nozzle.

(91)

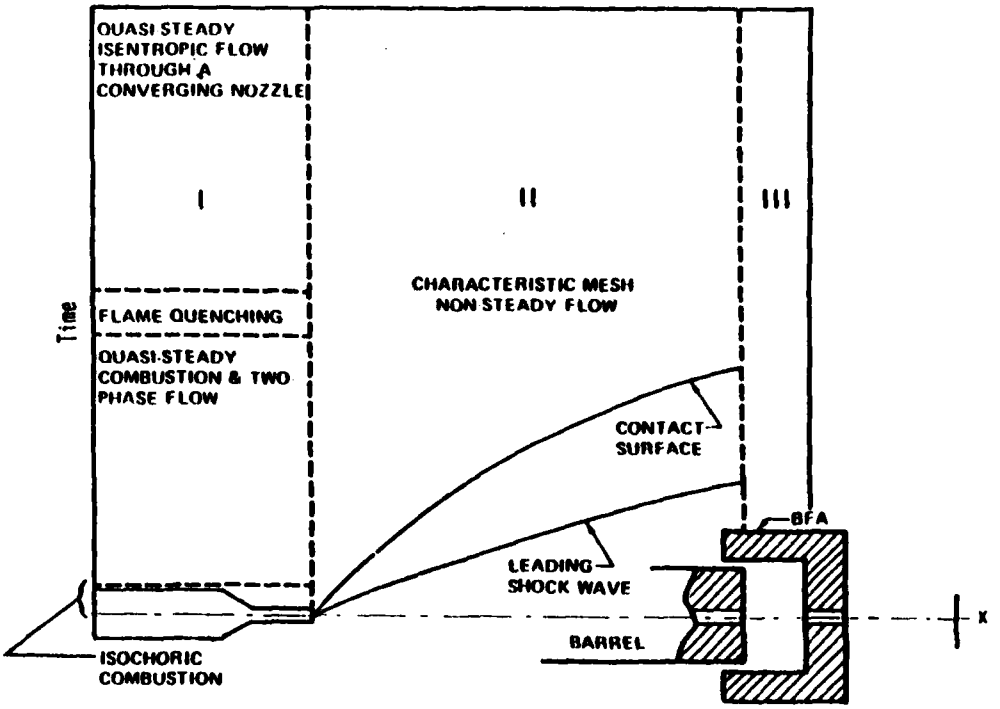

Figure 7. Three Phases of Blank Operation.

For Phase I a lumped ballistic model was used wherein all gas properties within the cartridge are assumed to be uniform. This phase also supplies the initial and boundary conditions for Phase II. Phase II describes the nonsteady flow in the barrel and includes the leading shock wave, contact surface and any compression or rarefaction waves. The method of characteristics [5] is used to solve the fluid flow equations for Phase II. Finally, Phase III defines the nonsteady flow entering the BFA [6], the pressure buildup in the BFA, and the motion of the bolt-barrel assembly. Interpolating along the characteristics at the muzzle, it is possible to determine the state of the gas entering the BFA. This flow is assumed to cease when the return shock forms.

Development of Equations

Phase I. An important parameter in the Phase I equations is the solid mass fraction ε [7]. For low values of loading density (characteristic of blank ammunition) the solid mass fraction ε may be approximated by

$$\varepsilon = \frac{\rho_p}{\rho_p + \rho_g} \qquad (2)$$

92

Accordingly, it is then possible to define a discharge coefficient C_d for the mixture.

$$C_d = \frac{\dot{m}}{APc} \qquad (3)$$

For a diabatic nozzel (constant temperature)

$$C_d = \frac{1}{\sqrt{F(T_c/T_o)\ (1-\varepsilon)\ e}} \qquad (4)$$

If one assumes an initial gas velocity (v_o) due to gas flow from the primer

$$C_d = \frac{\sqrt{v_o 2 + \frac{2FT_c}{T_o}\ (1-\varepsilon)\ (1/2 - \frac{v_o 2}{2F(T_c/T_o)\ (1-\varepsilon)})}}{F(T_c/T_o)\ (1-\varepsilon)\ e\ [1/2 - v_o 2/(2F(T_c/T_o)(1-\varepsilon)]} \qquad (5)$$

For perfect heat transfer between the phases

$$C_d = \left\{\frac{2\ C_T}{(1-\varepsilon)\ \frac{F\ T_c}{T_o}\left[2\ C_T - (1-\varepsilon)\ F/T_o\right]}\right\}^{1/2}\left[\frac{2\ C_T - 2\ (1-\varepsilon)\ F/T_o}{c\ C_T - (1-\varepsilon)\ F/T_o}\right]^{\frac{C_T\ T_o}{(1-\varepsilon)F}-1} \qquad (6)$$

For no heat transfer between the phases

$$C_d = \left[\frac{2\ \gamma\ T_o}{(\gamma-1)\ (1-\varepsilon)\ F\ T_c}\right]^{1/2}\left[\left(\frac{2}{\gamma+1}\right)^{\frac{2}{\gamma-1}} - \left(\frac{2}{\gamma+1}\right)^{\frac{\gamma+1}{\gamma-1}}\right]^{1/2} \qquad (7)$$

With these two parameters defined, it is now possible to formulate a set of 13 differential equations describing the interior ballistics (7, 8, 9) for Phase I during the quasisteady combustion and two-phase flow. A nondeterred, rolled-ball propellant is used in the propellant charge.

1. Burning rate equation is

$$\frac{d\delta}{dt} = BP_c^n \qquad (8)$$

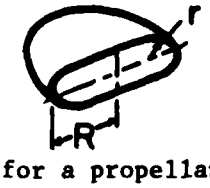

2. Rate of change of surface area for a propellant grain is derived by

$$\frac{d\ Si}{dt} = -2\pi\left[\pi(R-r) + 4\ (r-\delta)\right] BP_c^n \qquad (9)$$

(93)

3. Rate of change of grain volume equals

$$\frac{dVi}{dt} = -2\pi(R - r^2)^2 - 2\pi^2 (r - \delta)(R - r) - 4\pi (r - \delta)^2 BP_c^n \quad (10)$$

4. Rate of change of number of propellant grains in cartridge becomes

$$\frac{d N_h}{dt} = \frac{-\varepsilon \; C_d \; P_c \; A_c}{\rho s \; Vi}$$

5. Rate of discharge of propellant gas from cartridge case is

$$\frac{d C_o}{dt} = (1 - \varepsilon) P_c A_c C_d \quad (11)$$

6. Rate of increase of propellant gas in cartridge is solved by

$$\frac{d C_i}{dt} = \rho_s S_i N_B BP^n \quad (12)$$

7. Rate of change in amount of gas in cartridge is

$$\frac{d C_c}{dt} = \frac{d C_i}{dt} - \frac{d C_o}{dt} \quad (13)$$

8. Rate of change of gas temperature in cartridge is derived by

$$\frac{d T_c}{dt} = \frac{1}{C_c} \left[- \gamma T_c \frac{d C_o}{dt} + T_o \frac{d C_i}{dt} - T_c \frac{d C_c}{dt} \right] \quad (14)$$

9. Rate of change of gas pressure in the cartridge is

$$\frac{d P_c}{dt} = \frac{F}{T_o V_c^2} \left[V_c T_c \frac{d C_c}{dt} + V_c C_c \frac{d T_c}{dt} - C_c T_c \frac{d V_c}{dt} \right] +$$

$$\frac{Fig \; Cig}{Tig} \left[\frac{1}{V_c} \frac{d T_c}{dt} - \frac{T_c}{V_c^2} \frac{d V_c}{dt} \right] \quad (15)$$

10. Rate of change of gas density in cartridge case is found by

$$\frac{d \rho g}{dt} = \frac{T_o}{F} \frac{1}{T_c} \frac{d P_c}{dt} - \frac{P_c}{T_c^2} \frac{d T_c}{dt} \quad (16)$$

11. Rate of change of solid mass density is

$$\frac{d\rho_p}{dt} = \frac{- C_c P_c A_c - C_c}{U_o} \quad (17)$$

(94)

12. Rate of change of solid mass fraction is determined by

$$\frac{d\varepsilon}{dt} = \frac{\rho_g}{(\rho_p + \rho_g)} \frac{d\rho_p}{dt} - \frac{\rho_p}{(\rho_g + \rho_p)^2} \frac{d\rho_g}{dt} \qquad (18)$$

13. Rate change of free volume is

$$\frac{d\ V_c}{dt} = - \frac{u_o}{\rho_s} \frac{d\rho_p}{dt} - \eta \frac{d\ C_c}{dt} \qquad (19)$$

These 13 simultaneous differential equations were solved using a fourth order Runge-Kutta integration.

Flame Quenching: Flame quenching [10, 11] occurs when the pressure starts to drop rapidly. Subsequently, the flow is assumed to be quasisteady-insentropic as through a converging nozzle. Solution of these equations is shown in Figure 8 for the case where ε = variable ($v_o \neq 0$) and $\varepsilon = 0.5$ ($v_o \neq 0$). Figure 8 shows the experimental curve. Since a BFA was not used, no shock waves occurred.

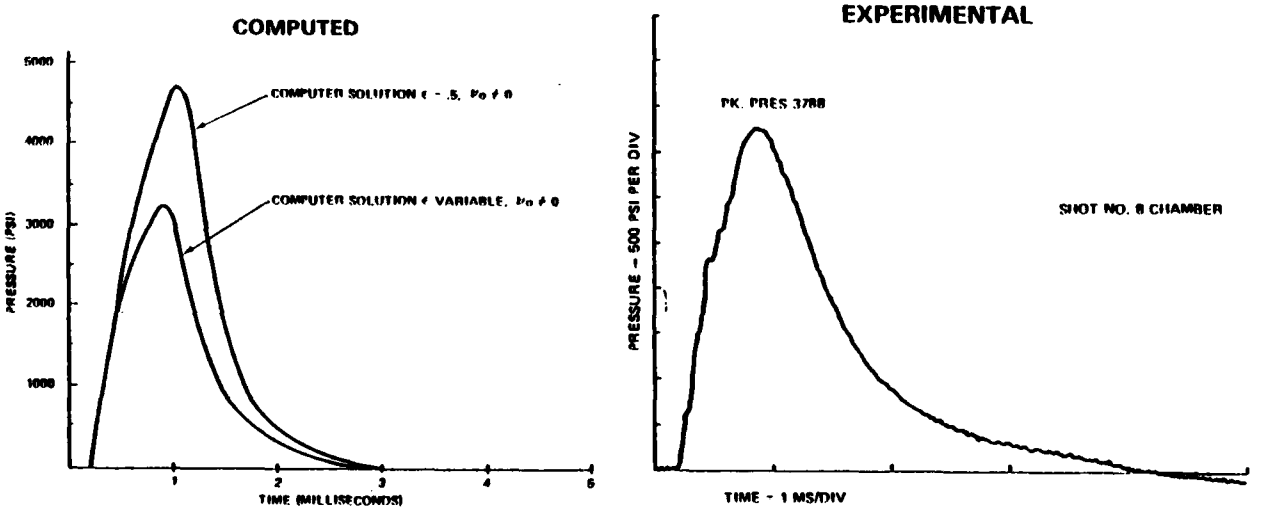

Figure 8. Chamber Pressure Versus Time.

(95)

Gas Leakage. Gas leakage in the BFA has a significant effect on the pressure. This leakage (Figure 9) occurs through the forward end of the BFA (A_{BFA}), through the clearance between the BFA and the barrel (A_{BLK}) and after the barrel has recoiled sufficiently through the vent port A_{PRT}.

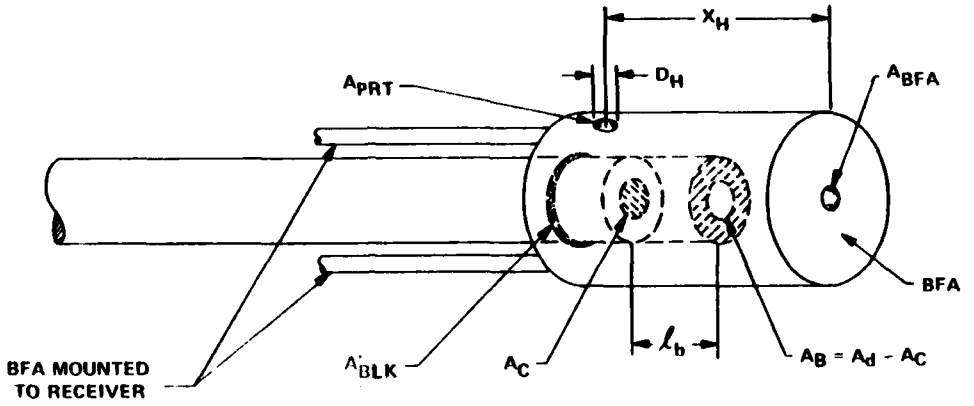

Figure 9. Cal .50 Barrel and BFA.

Equation of Motion. The equation of motion for the bolt-barrel assembly is determined from applied forces. Pressure in the BFA and in the cartridge case supply the accelerating forces. Five simultaneous differential equations must, however, be solved to determine this motion.

1. Equation of state for the BFA is solved by

$$\frac{d\,P_b}{dt} = \frac{mb^R}{U_b + A_d \ell b}\ \frac{d\,T_b}{dt} + \frac{R\,T_b}{U_b + A_d \ell b}\ \frac{dm_b}{dt} - \frac{RT_b\,A_d\,m_b}{(U_b + A_d \ell_b)^2}\ \frac{d\ell}{dt} \quad (20)$$

2. Energy equation for BFA becomes

$$\dot{m}e\ (1 - \beta)\left[C_p\,T_e + \frac{ve^2}{2gJ}\right]\left(1 - \frac{A_{BFA}}{A_c}\right) = \frac{P_b\,A_B}{J}\ \frac{d\ell b}{dt} + \frac{d}{dt}\ (m_b g C_v T_b) +$$

$$C_p\,T_b\,\dot{m}ob \quad (21)$$

or solving for gas temperature

$$\frac{d\,T_b}{dt} = \frac{\dot{m}e\ (1 - \beta)}{C_v\ mb}\left[C_p\,T_e + \frac{ve^2}{2gJ}\right]\left(1 - \frac{A_{BFA}}{A_c}\right) - \frac{P_b\,A_B}{gJC_v\,mb}\ \frac{d\ell b}{dt} -$$

$$\frac{C_p\,T_b\,\dot{m}ob}{mb\ C_v} - \frac{T_b\,\dot{m}b}{b} \quad (22)$$

(96)

where $\dot{m}_e$ is the rate at which gas enters the BFA and

$$\dot{m}ob = P_b \, (A_{BLK} + N_H \, A_{PRT}) \sqrt{\frac{\gamma}{R \, T_b} \left(\frac{2}{\gamma + 1}\right)^{\frac{\gamma + 1}{\gamma - 1}}} \qquad (23)$$

3. Equation of motion is found by

$$P_c \, A_c + P_b \, A_B - K_1 \, (\ell_b + X_o) - C_1 \, V - F_1 - F_2 = M_t \frac{dv}{dt} + 16.56 \, K_n \frac{dv}{dt} \qquad (24)$$

4. Conservation of propellant gas mass is computed by

$$\dot{m}_b = \dot{m}_e - \dot{m}_{ob} \qquad (25)$$

5. Equation of barrel-bolt displacement is

$$\frac{d\ell b}{dt} = V \qquad (26)$$

BFA Pressure-Time Curves. The computed and experimental pressure-time curve for the BFA and the experimental pressure-time curves are shown in Figure 10. The effect of the reverse shock wave is evidenced by the decrease in pressure following the peak. Meanwhile, the rise in pressure for the experimental curve following the peak is due to the arrival of the return shock from the breech.

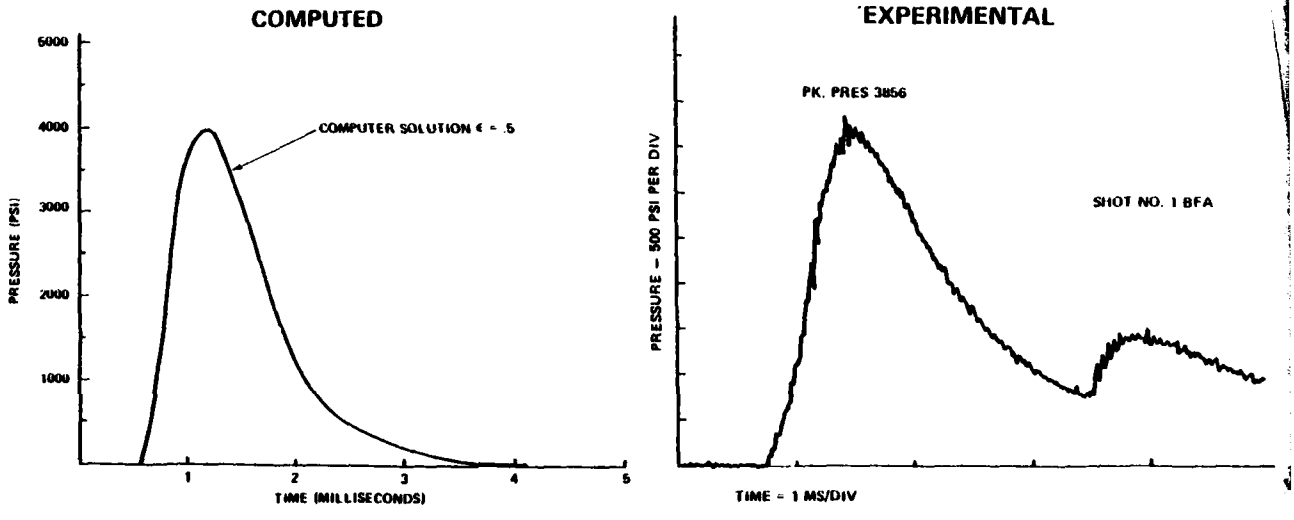

Figure 10. BFA Pressure Versus Time.

(97)

CONCLUSIONS

1. This model appears adequate for describing the quasisteady combustion and two phase flow from the .50 cal blank cartridge. It can also simulate the leading shock wave, compression wave and pressure buildup in the BFA.

2. The effective time-averaged solid mass fraction ε of about 0.5 seems reasonable for simulating the peak pressure in the cartridge case.

3. Quenching of the propellant flame immediately following the start of depressurization of the cartridge accounts for the shape of the pressure-time curve in the cartridge following peak pressure.

4. The pressure drop in the BFA chamber occurs when the first return shock wave forms and travels back toward the breech.

5. The method of characteristics can be used to solve equations describing nonsteady isentropic gas flow from cartridge case to BFA.

REFERENCES

1. R. F. Schwegler, "Evaluation of Two Blank Firing Attachments for the M2HB Caliber .50 Machine Gun," R-TR-76-022, General Thomas J. Rodman Laboratory (SARRI-LS-P), Rock Island Arsenal, Rock Island, IL 61201, June 1976.

2. H. E. Weidner , "M85 Math Model, Kinematic Model of the M85 Cal .50 Machine Gun," RETR-71-83, Small Arms Laboratory, US Army Weapons Command, Research and Engineering Directorate, Rock Island, IL, December 1971.

3. G. Rudinger, Nonsteady Duct Flow: Wave Diagram Analysis, Dover Publications, Inc., New York, NY 1969.

4. S. Goldstein, "Qualitative Investigation of the Functioning of 7.62MM Blank Ammunition," Frankford Arsenal Technical Note TN-1141, June 1969.

5. J. A. Owczarek, Fundamentals of Gas Dynamics, International Publishing Co., 1964.

6. S. Goldstein, "Study of the Flow Through the Pressure Port in a Gas Operated Small Arms Automatic Weapon," Frankford Arsenal Report FA-TR-76059, November 1976.

(98)

7. S. Goldstein, "Analytical Design Study of Caliber .50 Blank Ammunition and Weapon Interface," US Army Armament Research and Development Command, Technical Report (to be published).

8. S. Goldstein, "A Simplified Model For Predicting The Burning Rate and Thermochemical Properties of Deterred Rolled Ball Propellant," Frankford Arsenal Technical Note TN-1184, December 1973.

9. AMCP 706-150, Engineering Design Handbook, Ballistic Series, Interior Ballistics of Guns, US Army Materiel Command, February 1965.

10. C. L. Merkle, S. L. Turk, and M. Summerfield, "Exinguishment of Solid Propellants by Depressurization Effects of Propellant Parameters," AIAA Paper No. 69-176 (1969). Also AMS Report No. 880, Princeton University, Princeton, NJ 1969.

11. K. K. Kuo, "Review of Dynamic Buring of Solid Propellants In Gun and Rocket Propulsion Systems," 16th International Symposium On Combustion, pages 1177-1192, August 15-20, 1976.

LIST OF SYMBOLS (7)

A_d = cross-sectional area of BFA
C_P = specific heat for gas
C_S = specific heat for particles
C_T = $(1 - \varepsilon) C_P - \varepsilon C_S$
C_1 = spring damping constant
e = 2.718 -- base of natural logs
F = propellant impetus
F_1 = bolt receiver friction force
F_2 = barrel receiver friction-force
16.50 K_n = effect of number of rounds in the ammunition belt
K_1 = effective spring constant for bolt-barrel assembly
ℓ_b = travel of bolt-barrel assembly
m_b = mass of the gas in BFA
M_t = total moving mass
P_b = pressure in BFA
R = gas constant
T_c = gas temperature in the cartridge
T_o = isochoric adiabatic flame temperature
U_b = initial volume of BFA
X_o = initial compression of spring
η = gas covolume
ρ_g = density of gas in the mixture
ρ_p = density of solid particles in the mixture

(99)

(100)